Salphen metal complexes as potential anticancer agents: interaction profile and selectivity studies toward the three G-quadruplex units in the *KIT* promoter

Luisa D'Anna,[a] Simona Rubino,[a] Candida Pipitone,[b] Graziella Serio,[a] Carla Gentile,[a] Antonio Palumbo Piccionello,[a] Francesco Giannici,[b] Giampaolo Barone*[a] and Alessio Terenzi*[a]

DNA G-rich sequences can organize in four-stranded structures called G-quadruplexes (G4s). These motifs are enriched in significant sites within the human genomes, including telomeres and promoters of cancer related genes. For instance, *KIT* proto-oncogene promoter, associated with diverse cancers, contains three adjacent G4 units, namely, Kit2, SP, and Kit1. Aiming at finding new and selective G-quadruplex binders, we have synthesized and characterized five non-charged metal complexes of Pt(II), Pd(II), Ni(II), Cu(II) and Zn(II) of a chlorine substituted Salphen ligand. The crystal structure of the Pt(II) and Pd(II) complexes was determined by XRPD. FRET measurements indicated that Pt(II) and Pd(II) compounds stabilize Kit1 and Kit2 G4s but not SP, telomeric and double stranded DNA. Spectroscopic investigations (UV-Vis, circular dichroism and fluorescence) suggested the Cu(II) complex as the most G4-selective compound. Interestingly, docking simulations indicate that the synthesized compounds fit groove binding pockets of both Kit1 and Kit2 G4s. Moreover, they exhibited dose-dependent cytotoxic activity in MCF-7, HepG2 and Hela cancer cells.

1. Introduction

KIT proto-oncogene encodes for the membrane receptor protein tyrosine kinase KIT and is involved in several cellular functions, including proliferation. Dysregulations in KIT functions caused by different types of mutation are linked to the occurrence of several kinds of cancer including melanoma, breast cancer and gastrointestinal stromal tumors (GIST).[1]

Pharmacological treatment of these cancers often relies on receptor inhibiting agents which present significant side effects because of their low selectivity.[1] Therefore, it is of utmost importance to find new strategies that guide the synthesis of molecules that selectively and specifically recognize the target site, to act mostly in the cancer cells. Interfering on the regulation of *KIT* expression could represent a valid anticancer alternative to the targeting of the respective encoded protein. This strategy is nowadays possible thanks to the considerable progress in the development of DNA targeting drugs, especially considering non B-DNA motifs.

Single stranded G-rich DNA sequences, for example, can form four-stranded helices organized in stacked guanine tetrads connected by looping DNA bases and stabilized by a central monovalent ion channel (K^+, Na^+).[2,3] These structures, called G-quadruplexes (G4s), are enriched in highly conserved sequences located in relevant positions within the human genome, as telomers and promoters of cancer related genes.[2,3]

The *KIT* promoter contains three regions able to fold in G4 structures, known as Kit1, SP (or Kit*) and Kit2.[4,5] We and others have recently shown that Kit2 and SP G4s are functionally and structurally linked,[4,6] and that Kit1 has a more pronounced influence on the structural stability and the expression profile of the whole promoter.[4] With the aim to synthesize more selective anticancer drugs, based on G4 targeting, a good strategy could be to design a molecule able to preferentially binding with only one of these three sequences, preferably Kit1.[4]

Several molecules are reported to bind G4s.[7] Extended π-area to produce stacking on top of the G-tetrads, planar geometry and the presence of positively charged substituents to strengthen the interaction with the negative charges of the DNA motif, are among the main features of a suitable G4 binder. On the other hand, most of the G4 binders reported to date suffer from poor selectivity and, probably for that very reason, only two molecules capable of interacting with G4s entered clinical trials for human cancers to date.[8,9]

In the search for new and more effective DNA binders, special attention has been paid to metal complexes of Schiff base Salen- and Salphen-like ligands.[10–12] This class of molecules strongly and selectively binds G4s thanks to their general extended aromatic area, and to the presence of a metal center which improves the π–π stacking interaction with the G4 tetrad both making the ligand more electron deficient and organizing it in a suitable planar geometry.[11,13]

During the last years, our research group has considered different metal compounds as G4 binders.[10,11,14–16] Among them, metal complexes of Salphen-like ligands bearing positively charged substituents showed excellent properties and allowed us to study how the nature of the metal ion and the substituents influences the competitive binding with G4 and double-helical (B-DNA) structures. Certainly, the positive charge on the substituents promotes strong electrostatic interaction with DNA motifs but did

not always provide suitable G4 selectivity. Furthermore, in some cases, the ability of cationic metal complexes to cross the cytoplasmic membrane was dramatically reduced, forcing the need to use lipofectamine as a lipophilic carrier.[10]

As part of our continuous effort to improve the knowledge on metal-based compounds and their binding to G4 structures, we synthesized five non-charged metal complexes of Pt(II), Pd(II), Ni(II), Cu(II) and Zn(II) of a Salphen-like ligand bearing chlorine atoms as substituents. The compounds were characterized in solution and in the solid state with different techniques, including X-ray powder diffraction. The influence of the central metal ion was evaluated not only on the physical-chemical properties of the complexes but also on their binding to B-DNA and G4s structures with a special focus on the G4s of the *KIT* gene. We, therefore, studied the interaction of all the metal complexes with different DNA motifs, using different spectroscopic techniques supported by *in silico* docking calculations. Finally, the synthesized metal complexes were tested against three cancer cell lines (MCF-7, HepG2 and Hela) to evaluate their biological and potential anticancer activity.

2. Results and discussion

2.1. Synthesis and characterization

Although the five complexes **1**-**5** differ only in the coordinated metal ion, two different methods were necessary, with reaction conditions reported in Figure 1.

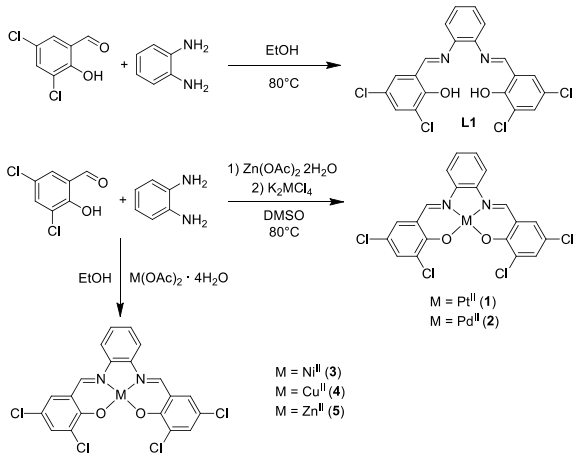

Figure 1. Synthetic routes for the preparation of ligand **L1** and compounds **1**-**5**

In particular, metal compounds **1** e **2**, with Pd(II) and Pt(II) metal centers, were synthesized through transmetalation of the Zn(II) analogue **5**, slightly modifying the methods developed for similar compounds.[17,18] In brief, after solubilizing the diamine, the aldehyde and $Zn(CH_3COO)_2$ in DMSO to obtain the Zn(II) complex *in situ*, Pd(II) and Pt(II) salts were directly added to the solution until a distinct change in color and formation of a precipitate was observed. The high Lewis acid character of the Zn(II) metal center allowed both the rapid formation of the Salphen complex **5**, in this case not isolated, and the preparation of thermodynamically more stable tetradentate structures with Pt(II) and Pd(II).
Ni(II), Cu(II) and Zn(II) complexes **3**, **4**, and **5**, respectively, were obtained by exploiting the simultaneous condensation of the salicylaldehyde and the diamine and the coordination of the metal center using the corresponding acetate salt, at room temperature and using EtOH as solvent. The synthesis of compound **5** was already reported, in different experimental conditions, by Kleij et al. who used the metal complex as a building block for the construction of supramolecular box assemblies.[19]
The synthetic pathway for all metal complexes did not involve the isolation of the ligand **L1**, which was synthesized and characterized for comparison purposes only.
Both ligand **L1** and its complexes **1**-**5** have been fully characterized by NMR, Mass and FT-IR. Compounds **1** and **2** structures were determined by X-ray Powder Diffraction. Agreement between experimental and calculated high resolution mass spectra is reported in Figure S1-S2 while ^{1}H NMR spectra are reported in Figure S3, with an overall purity >95% for all the tested compounds.

2.1.1. NMR and IR. The formation of the desired complexes was determined by ^{1}H NMR monitoring the diagnostic signal of the imine protons compared to the ligand (Figure S3).
For **L1**, the imine protons resonate at 9.01 ppm (DMSO-d6) while for Pt(II) and Pd(II) complexes **1** and **2** the corresponding signals were more downfield (9.36 and 9.69 ppm, respectively). Interestingly, the same signal is only slightly shifted for Zn(II) complex **5** and for the Ni(II) complex **3**, in contrast to what was reported for similar compounds, where the acidic Lewis character of the metal center affected much more the shifting of the imine signal.[10,17,20,21] The low solubility of the complexes hampered the recording of ^{13}C spectra except for Zn(II) compound **5**.

The formation of the metal complexes was also investigated by FT-IR spectroscopy. The -C=N stretching vibration at 1621 cm^{-1} in the spectrum of **L1** is shifted of about 10-15 cm^{-1} to lower wavenumbers in all metal compounds due to coordination (Figure S4). Metal coordination is further confirmed by the appearance of M-N and M-O stretching bands at 551 and 408 cm^{-1} (M=Pt), 544 and 402 cm^{-1} (M=Pd), 548 and 408 cm^{-1} (M=Ni), 537 and 370-353 cm^{-1} (M=Cu), 551 and 337 cm^{-1} (M=Zn), Figure S2.

2.1.2. X-ray Powder Diffraction

X-ray powder diffraction (XRPD) patterns were acquired for compounds **1** and **2**. The XRPD traces of compounds **1** and **2** indicate very well-crystallized powders with no amorphous contribution, and ab initio structure resolution was further carried out from indexing to Rietveld refinement. These two compounds are found to be isostructural, with monoclinic $P2_1/c$ (14) as the most probable space group (see Figure 2 for the crystal structure of compound **1**). Further details of data analysis are reported in the ESI along with the XPRD data (Figure S5, S6 and Table S1-S3).

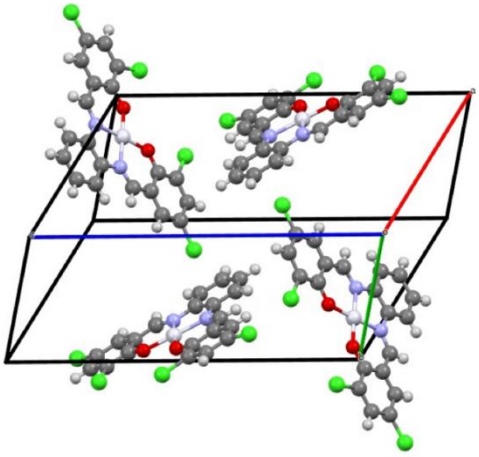

Figure 2. Crystal structure of compound **1**.

2.2. DNA-binding studies

The DNA sequences reported in Figure 3 and Table S4 were selected as targets of the synthesized metal complexes, and the DNA-binding was investigated by a series of spectroscopic techniques, including FRET, circular dichroism (CD), UV-Vis absorption and fluorescence.

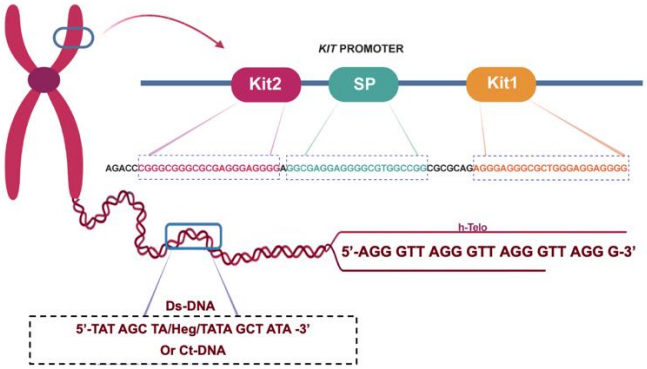

Figure 3. Sequences used for the DNA-binding studies. See also Table S4.

2.2.1. FRET. FRET (Fluorescence or Förster Resonance Energy Transfer) melting assay was performed to test the ability of the complexes to stabilize the secondary structure adopted by selected oligonucleotides properly modified with a fluorophore (FAM) and a quencher (TAMRA) at the 5' and 3' ends (see Table S4). In particular, we used a self-complementary sequence as B-DNA model (ds-DNA), three G4s from the *KIT* promoter (Kit2, Kit1 and SP) and the quadruplex forming sequence from the human telomer (h-Telo) (Figure 3).

The stabilization of the DNA secondary structure was evaluated by the increase of its melting temperature ($\Delta T_{1/2}$, where $T_{1/2}$ is the temperature at which normalized FAM emission is 0.5) caused by interaction with the metal complexes. We used two different [DNA]/[metal complex] ratios, 1/5 and 1/50 respectively, to test for possible concentration-dependent effects. At 1/5 ratio, all complexes showed no stabilization of ds-DNA and h-Telo and weak but promising interaction with both Kit2 and Kit1 G4s. In particular, Ni(II) compound **3** triggered a $\Delta T_{1/2}$ of approximately 4.0 and 7.0 °C when bound to Kit1 and Kit2 G4s, respectively (Figure S7 and Table S5). Even at 1/50 ratio, all complexes did not show stabilization of ds-DNA, regardless of the metal. Instead, they all exhibited good affinity toward G4s, confirming a certain degree of selectivity for this kind of DNA motif (Figure S8 and Table 1).

Table 1. $\Delta T_{1/2}$ values of 0.2 μM ds-DNA and G4s upon interaction with metal complexes at 10 μM concentration. Uncertainty is ≤ 0.5 for the $\Delta T_{1/2}$ reported.

	Metal	ds-DNA	h-Telo	Kit1	SP	Kit2
1	Pt	-1.6	1.6	16.8	0.8	15.8
2	Pd	-1.5	0.1	15.6	1.1	13.8
3	Ni	-1.1	2.7	8.5	3.3	7.7
4	Cu	-0.7	0.1	12.3	1.1	4.3
5	Zn	2.7	0.3	8.9	1.4	2.7

Among the three G4s from the *KIT* promoter, Kit1 and Kit2 resulted to be more affected by the interaction with the metal-based compounds while essentially no stabilization was observed for SP.
Pt(II) and Pd(II) complexes **1** and **2** exhibited the larger stabilization profiles with Kit1, triggering $\Delta T_{1/2}$ values of approximately 17 °C (Table 1 and Figure 4a) for **1**. Considering that compounds **1** and **2** showed solubility issues in aqueous solutions (*vide infra*), we performed the FRET assay also at lower concertation in order to exclude microprecipitation phenomena ([DNA]/[metal complex] ratio of 1/20, Figure S9). Pt(II) and Pd(II) complexes showed comparable $\Delta T_{1/2}$ values to the one obtained at 1/50 ratio, with the exception of compound **1** stabilization of Kit1 that dropped down to approximately 4 °C. Interestingly, Ni(II) compound **3**, which showed the larger stabilization of Kit2 at 1/5 ratio, did not modify its interaction profile at higher concentrations.

Encouraged by these results, we checked the selectivity for *KIT* G4 structures of the complexes with the best stabilization profile in solutions simulating physiological conditions. In details, we performed competitive FRET using labelled Kit1 in presence of compounds **1** and **2** and increasing the amount of calf-thymus DNA (Ct-DNA) as B-DNA model. The results showed that, despite the simultaneous presence of both DNA conformations, the thermal stabilization of Kit1 G4 is only slightly affected by the double-helical competitor (Figure 4b), as reported for other selective complexes.[22] In the case of **1** the effect of the competitor is minor and not concentration dependent, while the stabilization of Kit1 by **2** is influenced by the presence of Ct-DNA only at the higher concentrations used.
Overall, these results suggest a good affinity and selectivity of compounds **1** and **2** for Kit1 and Kit2 G4s. Therefore, we decided to further investigate the interaction of our compounds with these two G4 motifs.

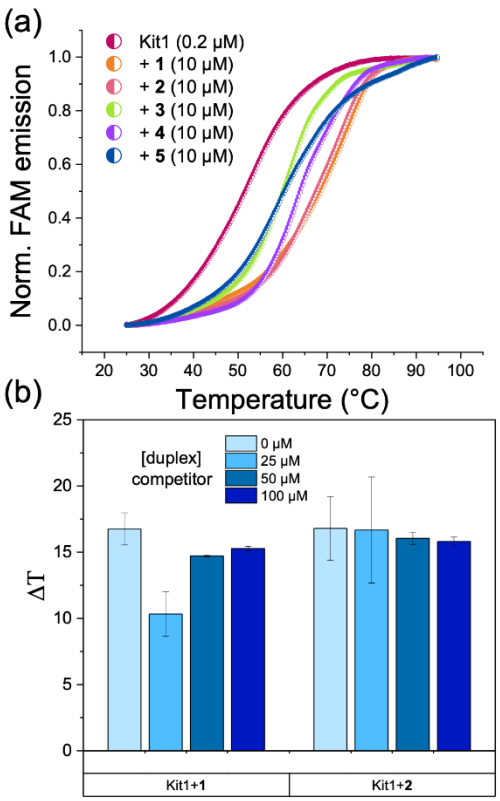

Figure 4. (a) FRET melting profiles of Kit1 G4 upon interaction with compounds **1**-**5** at the indicated concentrations. Buffer: 60 mM potassium cacodylate, pH 7.4. (b) Stabilization of Kit1 (0.2 µM) by **1** and **2** (10 µM) in the presence of increasing concentration of duplex DNA competitor (Ct-DNA). Concentration of G4s is reported per strand, and of Ct-DNA in bases. Buffer: 60 mM potassium cacodylate, pH 7.4

2.2.2. Circular dichroism and UV-Vis. CD is a useful spectroscopy technique that provides information about the topology of DNA structures. Kit1 and Kit2 sequences, in K^+ buffered solution, form parallel quadruplexes characterized by distinctive positive and negative bands at 263 and 241 nm, respectively.[4,23,24]
We checked how increasing amounts of **1**-**5** perturb Kit1 and Kit2 G4 conformations, and Ct-DNA one for comparison.

As shown in Figures S10-S12, the typical CD spectra of both B-DNA and quadruplexes, were not significantly modified after the interaction with all metal complexes, implying that the original topologies are preserved.

In order to get as much information as possible about the DNA binding properties and to determine the intrinsic binding constant (K_b) of the studied systems, we performed UV-Vis titrations of each complex in presence of increasing amount of Kit1, Kit2 and Ct-DNA (Figures S13-S15). In detail, we monitored changes in the characteristic band of the metal complex at around 400 nm, a region where DNA, both in its B- or G4 conformation, does not absorb. As a general trend, we noticed a hypochromic effect of the metal complexes absorption band due to the increasing DNA concentration, (Figures S13-S15), resulting in K_b values of around 10^4 M^{-1} (Table S6). Ni(II) and Cu(II) compounds **3** and **4** showed higher affinity for Kit2 G4 (Table S6) with K_b values of about 10^5. Interestingly, only for the Cu(II) compound **4**, no interaction was observed after B-DNA addition, while a distinct red shift appeared after the addition of Kit1 and Kit2, resulting in clear isosbestic points and confirming selectivity for G4 structures as observed in the FRET experiment. Unfortunately, it was not possible to obtain reliable quantitative data from UV-Vis titrations of compounds **1** and **2**, due to their low solubility in buffer and formation of precipitate after DNA addition. Considering the promising results coming from FRET analysis for these two compounds, higher binding constants values would be expected, and precipitation effects could be also due to the interaction strength with the DNA motifs tested in addition to their intrinsic poor solubility in buffer.

2.2.3. Fluorescence. Evaluation of the interaction between *KIT* G4s and our compounds was carried out also by fluorescence spectroscopy. We studied the ability of our compounds to emit light and how this emission could be influenced by the interaction with Kit1 and Kit2 G4s and Ct-DNA. Excitation of buffered solution of the metal complexes at wavelengths in the 250 – 500 nm range, allowed us to record 3D maps showing their characteristic emission bands (Figure S16). Despite differing only in the coordinated metal ion, the optical properties of compounds **1**-**5** are definitely different. Pt(II) and Pd(II) compounds **1** and **2** are not emissive in these experimental conditions. Both nickel and copper compounds **3** and **4**, when excited at 290 nm, share an emission band at about 450 nm but with different intensity, being the Cu(II) compound **4** more emissive. Zinc compound **5** emits

at higher intensity at almost all selected excitation wavelengths (as other zinc complexes of the same type[25]), with an emission band centered at around 550 nm (Figure S16).

Once selected the best excitation wavelength, we monitored if and how the emission of our compounds was affected by the addition of increasing amounts of DNA. As a general trend, we noticed a modest switch-OFF effect (≈20% reduction in fluorescence with 2.5 equivalents of DNA) when both B-DNA and the selected G4 sequences were added (Figure S17-S19), confirming the presence of an interaction with our metal-based compounds. Corroborating the UV-Vis titration results, only in the case of copper compound **4** no concentration dependent trend was observed following the addition of B-DNA.
To verify that our metal complexes have limited B-DNA binding capability we performed ethidium bromide (EB) displacement assay. EB is a well-known B-DNA intercalator which is strongly emissive only in the presence of the nucleic acid. A reduction in fluorescence of the EB-DNA system after titration with another molecule is associated with the displacement of EB, hence with a strong interaction of the tested compound with B-DNA. Interestingly, after titration of EB-DNA with compounds **1**-**5** (Figure S20), only a moderate reduction in fluorescence was observed (from about 4 to 10% at 1 eq. of metal complex per EB) if compared with Ni-Salnaph, a Schiff base metal complex synthesized previously by us and known to be a DNA intercalator.[26] Indeed, Ni-Salnaph caused a strong reduction in emission at 1 eq of metal complex per EB (≈60%) and even stronger when in excess, while the decrease in fluorescence resulted still limited when an excess of our compounds was used, confirming their limited B-DNA binding.

2.3. Molecular Docking

The NMR resolved structures of Kit1 (PDB id: 2O3M) and Kit2 (PDB id: 2KQG) were used as G4 models for docking studies. Looking at the most stable poses, in terms of binding energy (Figure 5 and S21), all metal complexes but compound **5** are bound within the groove binding pocket of the Kit1 structure, where two adenine residues (depicted in red in the figures) are located. Remarkably, of all the 50 possible poses, all of them are within this pocket for compounds **1**, **2** and **3** (49 out of 50 poses for the nickel compound **3**). The comparable behaviour of these three compounds is probably due to the planar geometry of the molecules given by the Pt(II), Pd(II) and Ni(II) d^8 metal centres. It is interesting to note that the cleft present in the Kit1 parallel structure, a unique feature among G4s, is particularly suitable for selective binding. Also compound **4** fits within Kit1 cleft in its best docking pose (Figure S21c), with another pose, shared with Ni(II) compound **3** (Figure 5), where the metal complex lays close to two cytosine residues (depicted in yellow) on top of the G4 tetrad. Zinc compound **5** best pose instead is directly on top of the G4 while in another pose it lays inside Kit1 binding pocket (Figure S21d).
Concerning Kit2 G4, basically all our compounds interact via π-π stacking with either the top or the down tetrads (Figure S22), a mode of binding expected for planar and aromatic compounds. Ni(II) compound **3**, in one of its two most stable poses, is the only one where the metal is perfectly centred to ideally continue the K^+ channel of the G4 (Figure S22c). Somewhat unexpectedly, besides top/end stacking, compounds **1**, **4** and **5** share a mode of binding where the metal complex is inserted in a groove pocket of Kit2 quadruplex (Figure 5b).

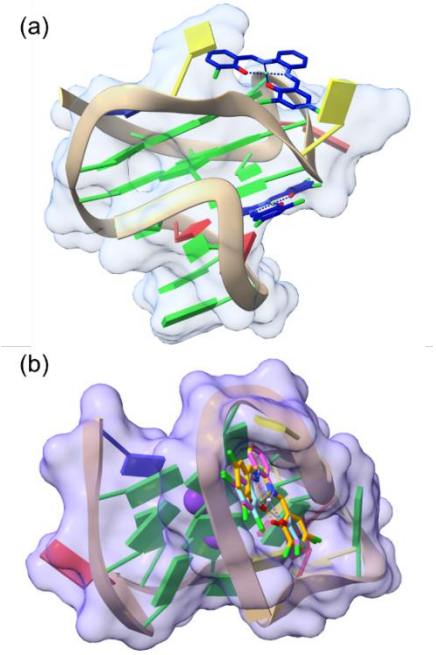

Figure 5. Cartoons showing possible binding sites of (a) **3** with Kit1 G4 (PDB id: 2O3M) and of **1** (cyan), **4** (magenta) and **5** (gold) with Kit2 (PDB id: 2KQG) G4 motifs. (Base colours: G = green, C = yellow, T = blue, A = red).

2.4. Biological Activity

Given the DNA binding properties of the synthesized metal complexes, we explored their potential anticancer activity against three human cancer cell lines. Cell growth inhibition tests against HeLa (human epithelial cervical cancer), HepG2 (human hepatocarcinoma), and MCF-7 (human epithelial breast cancer) were performed by exposing cells to test substances for 48 h. In Table 2 the GI_{50} (50% of growth inhibition) values for the compounds are presented.

Stock solutions of compounds **1**-**5**, were prepared in DMSO. Considering that in every experiment DMSO concentration never exceeded 0.25% due to its intrinsic toxicity, and that the compounds showed different solubility in this solvent (generally poor), the concentration ranges used for the cytotoxicity test vary from one compound to another and it is reported in Table 2. For compound **5**, the most soluble in DMSO, we were able to measure a GI_{50} value for all the three cell lines. On the contrary, compounds **1**-**4** were tested at very low concentrations, even nanomolar for compounds **1** and **2**. In these experimental conditions we are unable to detect any activity for compound **2** and it was not always possible to measure a GI_{50} value for compounds **1**, **3**, and **4**. HeLa cells, which cell cycle is faster compared to the other two tested cell lines, were more sensitive to treatment with compounds **1**, **4**, and **5**. In particular, very high activity was assessed on this cell line for compound **1** with a GI_{50} value of 0.7 μM. Interestingly, in our experimental conditions, the Ni(II) complex **3** resulted active exclusively against HepG2 cells.

Table 2. Antiproliferative activity at 48 hrs of complexes **1**-**5** against HeLa, MCF-7, and HepG2 cell lines expressed as GI_{50} values [GI_{50} ± SE (μM)].

	HeLa	**MCF-7**	**HepG2**
1 (775 – 155 nM)	0.72 ± 0.06	n.a.	n.a.
2 (3.3 – 1.0 μM)	n.a.	n.a.	n.a.
3 (7.1 – 1.5 μM)	n.a.	n.a.	5.97 ±0.11
4 (4.9 – 1. μM)	4.12 ± 0.37	3.90 ± 0.47	n.a.
5 (27.0 – 2.7 μM)	6.60 ± 0.52	11.28 ± 0.69	9.13 ± 0.56

3. Conclusions

We have synthesized and thoroughly characterized five non-charged metal complexes of Pt(II), Pd(II), Ni(II), Cu(II) and Zn(II) of chlorine substituted Salphen ligand. The zinc compound **5**[19] was used as starting point for the transmetallation of Pt(II) and Pd(II) metal centers to obtain compound **1** and **2**, respectively, while the synthesis of Ni(II) and Cu(II) complexes **3** and **4** went smooth without need of transmetallation. The crystal structures of **1** and **2**, obtained by XRPD, revealed a square planar coordination geometry as expected for tetracoordinated d^8 metal complexes.

The binding of the synthesized compounds with duplex and G-quadruplex DNA in solution was investigated by a range of spectroscopic techniques. FRET experiments, also in presence of B-DNA as competitor, revealed stabilization of two of the three G4 structures present in proto-oncogene promoter *KIT* by **1**, **2** and, to a lesser extent by **4**. The last compound confirmed to have preference for G4 structures in UV-Vis titrations, while CD studies confirmed that the secondary structures of both B-DNA and G4s were not influenced by the interaction with the tested compounds. Metal complexes **3**, **4** and **5** resulted to be emissive, an important aspect for *in cellulo* localization. Also fluorescence emission confirmed the selectivity of the Cu(II) compound **4** for Kit1 and Kit2 G4s. EB displacement assay confirmed an overall limited B-DNA binding ability of all the metal complexes tested. Compounds **1** and **2** were not tested by UV-Vis because of their poor solubility, neither by fluorescence since they were not emissive. Nonetheless, they showed the most promising results in the FRET analysis, where lower concentrations were required to stabilize the considered G4s. Furthermore, compound **1** showed a nanomolar activity when tested against HeLa cells, an impressive result considering the low range of concentration used for the last study. When solubility allowed an increase in concentration, compound **3**, **4** and **5** resulted to be active in the low micromolar range also against MCF-7 and HepG2 cancer cell lines.

Such results find support in molecular docking: metal compounds **1**-**4** fit within the special groove binding pocket of Kit1. Interestingly, **1**, **4** and **5**, besides interacting via top/end stacking, as expected for this class of compounds, fit a groove pocket of the Kit2 quadruplex, corroborating the UV-Vis and fluorescence results for the Cu(II) complex.

Overall, even if our metal complexes can be considered modest G4 binders in general terms (other molecules, including Salphen metal compounds synthesized by us and others,[10,27,28] induce higher $\Delta T_{1/2}$ values at lower concentration in FRET analysis), they showed a promising preference for the *KIT* G4s vs. B-DNA as confirmed by competitive experiments and EB displacement assay, as well as a good cytotoxicity profile when tested in cancer cells. Following the obtained results, our laboratory is working on the synthesis of complexes of the same class with better solubility, higher binding ability but with the same degree of selectivity of the compounds herein presented.

4. Experimental

4.1. General

Chemicals and solvents were used in commercial grade (Sigma Aldrich and Thermo Fisher Scientific) from freshly opened containers without further purification. Proton and Carbon NMR spectra were recorded on Brucker AC-E series 300 MHz and on Bruker AC-E series 400 MHz. Mass spectrometry experiments were carried out on Agilent 6540 QTOF LC/MS. IR analysis was carried out by FT-IR Bruker Vertex 70v spectrometer. Fluorescence spectra were recorded by Jasco spectrofluorometer FP-8300. IR analysis was carried out by FT-IR Bruker Vertex 70v spectrometer.
Buffers were prepared using MilliQ water and final pH values were measured by CREASON pH meter-GLP.

4.2. Synthetic procedures

Synthesis of the ligand (L1). A solution of 3,5-dichlorosalicylaldehyde (502.4 mg, 2.63 mmol) and 1,2-phenylendiamine (140 mg, 1.3 mmol) in EtOH was refluxed for 4 hours and then left at room temperature overnight. The bright yellow precipitate was filtered and washed by cold distilled water, ethanol and diethyl ether.
^{1}H NMR (300 MHz, DMSO) δ 13.88 (s, 1H, OH), 9.02 (s, 1H, N=CH), 7.81 (dd, 3H, ArCH), 7.52. 7.76 (m, 3H, ArCH). ESI-MS (m/z) calculated for $[M+H]^+$ 454.9698, found 454.9698.

Synthesis of metal complexes. Complexes **1** and **2** were synthesized, under inert atmosphere, slightly modifying the transmetalation method used for similar compounds.[17,18] Complexes **3**, **4** and **5** were synthesized in a one-pot reaction where the salicylaldehyde, the diamine and the metal salt are mixed together without isolating the ligand, as reported by us for compounds of the same family.[10,11,20] The corresponding IR spectra are reported in Figure S2.

Pt(II) complex (1). To a 1,2-phenilendiamine (10.81 mg, 0.1 mmol) and 3,5-dichlorosalicylaldehyde (38.22 mg, 0.2 mmol) solution in DMSO (1 mL), $Zn(CH_3COO)_2$ (24.95 mg, 0.1 mmol) was added. The resulting solution was stirred at 80 °C for 2 hours before adding K_2PtCl_4 (45.7 mg,0.1 mmol). The mixture was left under stirring for 72 hours. The precipitate was washed with methanol (30 mL) to afford **1** as red crystalline solid (39.4 mg, 77% yield).
^{1}H NMR (400 MHz, DMSO-d6) δ 9.28 (s, 1H), 8.31 (dd, J = 6.4, 3.3 Hz, 1H), 7.86 (d, J = 2.8 Hz, 1H), 7.79 (d, J = 2.8 Hz, 1H), 7.55 (dd, J = 6.4, 2.9 Hz, 1H). ESI-MS calculated for $[M+Na]^+$ 668.9012, found 668.9012.

Pd(II) complex (2). This compound was prepared as for **1**, but K_2PdCl_4 (32.36 mg,0.1 mmol) was added instead of the Pt(II) salt. The mixture was left under stirring for 24 hours. The precipitate was washed with methanol (30 mL) to afford **2** as orange crystalline solid (42.2 mg, 68.7% yield).
^{1}H NMR (400 MHz, DMSO-d6) δ 9.61 (s, 1H), 8.39 (dd, 1H), 7.98 (d, J = 2.5 Hz, 1H), 7.92 (d, J = 2.3 Hz, 1H), 7.53 (dd, 1H). ESI-MS calculated for $[M+Na]^+$ 580.8409, found 580.8419.

Ni(II) complex (3). A solution of 3,5-dichlorosalicylaldehyde (191.1 mg, 1 mmol) and 1,2-phenilendiamine (54.07 mg, 0.5 mmol) in ethanol was stirred for 30 minutes at room temperature before adding $Ni(CH_3COO)_2{\cdot}4H_2O$ (136.87 mg, 0.5 mmol) previously dissolved in the minimum amount of H_2O. The mixture was left stirring for 4 hrs. The resulting precipitate was washed with cold water, ethanol and diethyl ether to afford **3** as a red solid (84.5 mg, 82.7% yield).
^{1}H NMR (300 MHz, DMSO-d6) δ 9.01 (s, 1H), 7.80 (d, 2.6 Hz, 1H), 7.75 (d, 2.6Hz, 1H) 7.62 – 7.39 (m, 2H).); ESI-MS calculated for $[M+Na]^+$ 532.8710, found 532.8719.

Cu(II) complex (4). This compound was prepared as for **3**, but $Cu(CH_3COO)_2{\cdot}4H_2O$ (99.82 mg, 0.5 mmol) was used instead of the Ni(II) salt. The mixture was left stirring for 4 hrs. The resulting precipitate was washed with cold water, ethanol and diethyl ether to afford **4** as a green solid (86.8 mg, 74.5 yield).
ESI-MS (m/z) calculated for $[M+Na]^+$ 537.8659, found 537.8656;

Zn(II) complex (5). This compound was prepared as for **3**, but $Zn(CH_3COO)_2{\cdot}4H_2O$ (109.74 mg, 0.5 mmol) was used instead of the Ni(II) salt. The mixture was left stirring for 4 hrs. The resulting precipitate was washed with cold water, ethanol and diethyl ether to afford **5** as a yellow solid (99.8 mg, 88.7 yield).
^{1}H NMR (300 MHz, DMSO-d6) δ 9.03 (s, 1H), 7.88 (dt, J = 6.2, 3.5 Hz, 1H), 7.55 (q, J = 2.9 Hz, 2H), 7.46 (s, 1H); ^{13}C NMR (400 MHz, DMSO-d6): (δ, ppm) 164.50 (-CH=N), 139.22 (C-Ar), 133.56 (C-Ar), 132.43(C-Ar), 128.21 (C-Ar), 126.85 (C-Ar), 120.56 (C-Ar), 117.07 (C-Ar), 114.59 (C-Ar). ESI-MS (m/z) calculated for $[2M+Na]^+$ 1056.7392, found 1056.7395.

4.3. X-ray Powder Diffraction

X-ray diffraction patterns were collected on powdered samples in Bragg-Brentano geometry with a Rigaku Miniflex using Ni-filtered Cu K_α radiation, a 1.25° incident beam slit, beam knife and a 1D silicon strip detector. XRPD data were acquired between 5 and 70°

2θ. Ab initio structure resolution was performed with Topas Academic,[29] on compounds **1** and **2**. During simulated annealing and Rietveld refinement, rigid body constraints were imposed on bond lengths and angles with a Z-matrix formalism using database data on similar compounds.

4.4. Interaction with G4 and B-DNA in solution

All absorption and emission spectra were recorded for freshly prepared solution of the samples.

4.4.1. DNA sequences for binding studies. Lyophilized calf thymus DNA (Ct-DNA) was purchased from Sigma-Aldrich and resuspended in 1.0 mM Tris-HCl (tris-hydroxymethyl-aminomethane) pH=7.5. Final DNA concentration in bases was determined by UV spectrophotometry measuring the absorbance at 260 nm and using 6600 M^{-1} cm^{-1} as molar absorption coefficient. The oligodeoxynucleotides (ODNs) reported in Figure 3 and Table S4 were purchased from Sigma Aldrich and IDT (Integrated DNA Technologies) in HPLC purity grade. Concentrations are reported per strand or per bases depending on the experiment, as indicated in the captions. For the determination of binding constants, concentrations are always per bases.

4.4.2. FRET melting assay. FRET experiments were performed on a 96-well format Applied Biosystems™ QuantStudio 6 PCR cycler with a FAM (6-carboxyfluorescein) filter. The ODNs, with FAM and TAMRA (6-carboxy-tetramethylrhodamine) probes, stock solutions were diluted to the desired concentration using 60 mM potassium cacodylate buffer (pH 7.4). Then they were folded in their B-DNA or G4 topology heating the solutions to 95 ^{O}C for 5 min, followed by slowly cooling to room temperature overnight. In the final mixes, ODNs final concentration was set to 0.2 μM (total volume of 30 μl). Metal complexes were dissolved in DMSO to give 1 mM stock solution and further diluted with the buffer reaching a total percentage of DMSO never above 0.1 %.
The melting temperature of Kit1 G4 (at 0.2 μM) stabilised by compounds **1** and **2** was also monitored in a competition assay in the presence of increasing amount of the non-fluorescent B-DNA structure Ct-DNA. FAM emission data were collected in duplicate in the range 25-95 ^{O}C (with a ramp of 1 ^{O}C every 30 s). To compare different sets of data, emission data were normalized from 0 to 1.[30]

4.4.3. UV-Vis absorption and Circular dichroism. Uv-Vis spectra were recorded on a double-beam spectrophotometer Cary 1E at room temperature and adding increasing amounts of G4-DNA or B-DNA to a solution of **1-5** at constant concentration. The titrations were carried out by adding increasing amounts of DNA solution to the metal complex solution. To guarantee that during the titration the concentration of the selected metal complex remained unaltered, for each addition of the DNA solution the same volume of a double-concentrated metal complex solution was added. CD spectra were recorded on a spectropolarimeter Jasco J-715 at 25°C, adding increasing amounts of metal complexes (**1-5**) to a solution of DNA at constant concentration. The parameters were the following: range 400-220 nm, response: 0.5s, accumulation: 4, speed 200 nm/min.
For both CD and UV experiments, ODNs were resuspended in Tris-KCl buffer (50 mM Tris-HCl, 100 mM KCl, pH 7.4) to yield a 100 μM stock solution expressed in strand units. G4 folding was obtained as described in the FRET section.
K_b values were obtained by fitting the UV data to a reciprocal plot of $C_{DNA}/|\varepsilon_a-\varepsilon_f|$ vs. C_{DNA} using the equation $C_{DNA}/|\varepsilon_a-\varepsilon_f| = C_{DNA}/|\varepsilon_b-\varepsilon_f| + 1/(|\varepsilon_b-\varepsilon_f| \times K_b)$,[31] where C_{DNA} is total analytical DNA concentration expressed in bases, $\varepsilon_a = A_{observed}/[\text{Metal Complex}]$, ε_b is the extinction coefficient of the DNA bound metal complex, and ε_f is the extinction coefficient of the free metal complex.

4.4.4. Fluorescence. Fluorescence studies were carried out on a JASCO FP-8300, Rev. 1.00, at room temperature adding increasing amounts of G4s and B-DNA and using the following parameters: response: 0.5 sec, Measurement range: 315 – 750 nm for **3, 4** spectra, 325 – 750 nm for **5** spectra, excitation wavelength: 300 nm (**3, 4**), 310 nm (**5**), sensitivity: medium; data interval: 1 nm, scan speed: 1000 nm/min. Spectra were recorded at room temperature with excitation and emission slit widths as reported in the captions of the corresponding pictures.

4.5. Molecular docking

Structures of the metal complexes were fully optimized by DFT calculations implemented in the Gaussian16 program package,[32] using the m06l functional,[33] the LANL2TZ(f) pseudopotential basis set for metal atoms,[34] and the 6-311G(d,p) basis set for the other atoms.[35]
Autodock Tools 1.5.6 [36] was used to prepare the receptors Kit1 (PDB id: 2O3M), Kit2 (PDB id: 2KQG) and the metal complexes as pdqt files. A grid box large enough to include all the receptor binding sites (blind-docking) was created. In particular, grid size for 2O3M was set to 60 Å × 60 Å × 60 Å points with grid spacing of 0.5 Å and a grid center of -1.084, 4.144, -1.226 xyz-coordinates. Grid size for 2KQG was set to 60 Å × 60 Å × 60 Å points with grid spacing of 0.5 Å and a grid center of -1.077, 1.89, -0.165 xyz-coordinates Figures were rendered using ChimeraX.[37]

Molecular docking was performed using AutoDock 4.2.[36] Docking was ran using the Lamarckian Genetic Algorithm with all the parameters set as following. Estimated free energies of binding are expressed in kcal/mol.

4.6. Biological Activity

4.6.1. Chemicals and reagents. 2,5-diphenyl-3,-(4,5-dimethyl-2-thiazolyl) tetrazolium bromide (MTT) and dimethyl sulfoxide (DMSO) were obtained from Sigma Aldrich (St. Louis, MO, USA). Dulbecco's Modiefied Eagle's Medium-high glucose (DMEM), RPMI medium, fetal bovine serum (FBS), phosphate buffered saline (PBS), L-glutamine solution (200 mM), trypsin-EDTA solution (170000 U/l trypsin and 0.2 g/l EDTA) and penicillin-streptomycin solution (10000 U/ml penicillin and 10 mg/ml streptomycin) were purchased from Lonza (Verviers, Belgium).

Cell culture. The tumor cell lines HeLa (human epithelial cervical cancer), HepG2 (human hepatocarcinoma), and MCF-7 (human epithelial breast cancer) were obtained from American Type Culture Collection (ATCC) (Rockville, MD, USA). Monolayers of cells were cultured and incubated in a humidified atmosphere with 5% CO_2 at 37 °C. DMEM was used as culture medium for MCF-7 cells while RPMI was employed for HeLa and HepG2 cells. Both mediums were supplemented with 5% FBS, 2 mM L-glutamine, 50 IU/ml penicillin, and 50 µg/ml streptomycin. The cells were regularly cultured in 75 cm^2 culture flasks and collected using trypsin-EDTA. MTT assay was carried out using exponentially growing cells.

4.6.2. Antiproliferative Activity. To evaluate the growth inhibition activity against tumor cell lines, for all the synthesized complexes MTT assay was performed. This assay, a quantification of cell metabolic activity that quite effective estimate cell proliferation, is based on the protocol first described by Mosmann,[38] and was assessed as previously described.[39]
The cells were seeded into a series of standard 96-well plates at a plating density depending on the doubling times of individual cell line. HeLa, HepG2, and MCF-7 cells were seeded at 1.0×10^4, 2.5×10^4, and 1.5×10^4 cells/cm^2 respectively. Cells were incubated under 5% CO_2 at 37 ° C for 24 h. The different metal complex stock solutions (**1**: 0.31 mM, **2**: 1.32 mM, **3**: 2.84 mM, **4**: 1.96 mM, **5**: 10.80 mM) were prepared by dissolving the metal-base compound powders in DMSO. Working solutions were freshly prepared by dilutions of the stock solution in serum-free medium. In each experiment, DMSO concentration never exceeded 0.25% and for this reason the five metal complexes were tested using different concentration ranges (**1**: 775 - 155 nM; **2**: 3.3- 1.0 µM; **3**: 7.0-1.5 µM; **4**: 4.9-1.5 µM; **5**: 27.0- 1.5 µM). After 24 h from seeding, the metal complex solutions at different concentrations were added to the appropriate wells and the cells were incubated for 48 h, without replacement of the medium. Culture medium with 0.25% DMSO was used as control. After the incubation time, cells were washed and 100 µL of 0.5 mg/mL MTT solution was added. The medium was discarded after a 4 h incubation at 37 °C and formazan blue formed in the cells was dissolved in DMSO. The absorbance (OD, optical density) at 570 nm of MTT-formazan was measured in a microplate reader. As the absorbance is directly proportional to the number of metabolically active cells, the percentage of growth (PG) to respect untreated cell control, for each tested compound concentrations, were calculated according to one of the following two expressions:
if $(OD_{test} - OD_{tzero}) \geq 0$, then $PG = 100 \times (OD_{test} - OD_{tzero})/(OD_{ctr} - OD_{tzero})$; if $(OD_{test} - OD_{tzero}) < 0$, then $PG = 100 \times (OD_{test} - OD_{tzero})/OD_{tzero}$, where: OD_{test} is the average of optical density after cell exposure to the tested compound for a chosen period of time; OD_{tzero} is the average of optical density before the addition of the tested compound; OD_{ctr} is the average of optical density after the chosen period of time with no exposure of cells to the tested compound.
The concentration necessary for 50% of growth inhibition (GI_{50}) for each metal-complex was calculated from concentration−response (PG) curves using linear regression analysis by fitting the test concentrations that give PG values above and below the reference value (i.e. 50%). If, however, for a given cell line all of the tested concentrations produced PGs exceeding the respective reference level of effect (PG value of 50), then the results were reported as n.a. (not applicable). Each result was the mean value of three separate experiments performed in quadruplicate.

5. Author Contributions

Luisa D'Anna: investigation, methodology, formal analysis, visualization, writing – original draft. Simona Rubino: investigation, methodology; Candida Pipitone: investigation, methodology; Graziella Serio: investigation, methodology; Carla Gentile: investigation, methodology; Antonio Palumbo Piccionello: investigation, methodology; Francesco Giannici: investigation, methodology, visualization; Giampaolo Barone: conceptualization; writing - review & editing; Alessio Terenzi: conceptualization; writing – original draft, methodology, formal analysis; supervision.

6. Conflicts of interest

The authors declare no conflict of interest

7. Acknowledgements

We thank Prof. N. Masciocchi (University of Insubria, Italy) for advice on crystal structure refinement and useful discussion and Simona Di Maria for support in the synthetic work. FRET experiments were performed at AteN Center – Università di Palermo.

8. Notes and references

1 S. Pathania, O. T. Pentikäinen and P. K. Singh, *Biochimica et Biophysica Acta (BBA) - Reviews on Cancer*, 2021, **1876**, 188631.
2 R. Hänsel-Hertsch, M. Di Antonio and S. Balasubramanian, *Nat Rev Mol Cell Biol*, 2017, **18**, 279–284.
3 D. Varshney, J. Spiegel, K. Zyner, D. Tannahill and S. Balasubramanian, *Nat Rev Mol Cell Biol*, 2020, **21**, 459–474.
4 C. Ducani, G. Bernardinelli, B. Högberg, B. K. Keppler and A. Terenzi, *J. Am. Chem. Soc.*, 2019, **141**, 10205–10213.
5 A. Kotar, R. Rigo, C. Sissi and J. Plavec, *Nucleic Acids Research*, 2019, **47**, 2641–2653.
6 R. Rigo and C. Sissi, *Biochemistry*, 2017, **56**, 4309–4312.
7 S. Neidle, *Nat Rev Chem*, 2017, **1**, 0041.
8 D. Drygin, A. Siddiqui-Jain, S. O'Brien, M. Schwaebe, A. Lin, J. Bliesath, C. B. Ho, C. Proffitt, K. Trent, J. P. Whitten, J. K. C. Lim, D. Von Hoff, K. Anderes and W. G. Rice, *Cancer Research*, 2009, **69**, 7653–7661.
9 H. Xu, M. Di Antonio, S. McKinney, V. Mathew, B. Ho, N. J. O'Neil, N. D. Santos, J. Silvester, V. Wei, J. Garcia, F. Kabeer, D. Lai, P. Soriano, J. Banáth, D. S. Chiu, D. Yap, D. D. Le, F. B. Ye, A. Zhang, K. Thu, J. Soong, S. Lin, A. H. C. Tsai, T. Osako, T. Algara, D. N. Saunders, J. Wong, J. Xian, M. B. Bally, J. D. Brenton, G. W. Brown, S. P. Shah, D. Cescon, T. W. Mak, C. Caldas, P. C. Stirling, P. Hieter, S. Balasubramanian and S. Aparicio, *Nat Commun*, 2017, **8**, 14432.
10 A. Terenzi, D. Lötsch, S. van Schoonhoven, A. Roller, C. R. Kowol, W. Berger, B. K. Keppler and G. Barone, *Dalton Trans.*, 2016, **45**, 7758–7767.
11 G. Farine, C. Migliore, A. Terenzi, F. Lo Celso, A. Santoro, G. Bruno, R. Bonsignore and G. Barone, *Eur. J. Inorg. Chem.*, 2021, **2021**, 1332–1336.
12 T. Kench and R. Vilar, in *Annual Reports in Medicinal Chemistry*, Elsevier, 2020, vol. 54, pp. 485–515.
13 N. H. Campbell, N. H. A. Karim, G. N. Parkinson, M. Gunaratnam, V. Petrucci, A. K. Todd, R. Vilar and S. Neidle, *J. Med. Chem.*, 2012, **55**, 209–222.
14 R. Bonsignore, F. Russo, A. Terenzi, A. Spinello, A. Lauria, G. Gennaro, A. M. Almerico, B. K. Keppler and G. Barone, *Journal of Inorganic Biochemistry*, 2018, **178**, 106–114.
15 O. Domarco, C. Kieler, C. Pirker, C. Dinhof, B. Englinger, J. M. Reisecker, G. Timelthaler, M. D. García, C. Peinador, B. K. Keppler, W. Berger and A. Terenzi, *Angew. Chem. Int. Ed.*, 2019, **58**, 8007–8012.
16 O. Domarco, D. Lötsch, J. Schreiber, C. Dinhof, S. Van Schoonhoven, M. D. García, C. Peinador, B. K. Keppler, W. Berger and A. Terenzi, *Dalton Trans.*, 2017, **46**, 329–332.
17 E. C. Escudero-Adán, J. Benet-Buchholz and A. W. Kleij, *Inorg. Chem.*, 2007, **46**, 7265–7267.
18 T. Kench, P. A. Summers, M. K. Kuimova, J. E. M. Lewis and R. Vilar, *Angew. Chem. Int. Ed.*, 2021, **60**, 10928–10934.
19 A. W. Kleij, M. Kuil, D. M. Tooke, M. Lutz, A. L. Spek and J. N. H. Reek, *Chem. Eur. J.*, 2005, **11**, 4743–4750.
20 A. Terenzi, C. Ducani, L. Male, G. Barone and M. J. Hannon, *Dalton Trans.*, 2013, **42**, 11220.
21 A. Lauria, R. Bonsignore, A. Terenzi, A. Spinello, F. Giannici, A. Longo, A. M. Almerico and G. Barone, *Dalton Trans.*, 2014, **43**, 6108.
22 C. L. Ruehl, A. H. M. Lim, T. Kench, D. J. Mann and R. Vilar, *Chem. Eur. J.*, 2019, **25**, 9691–9700.
23 H. Fernando, A. P. Reszka, J. Huppert, S. Ladame, S. Rankin, A. R. Venkitaraman, S. Neidle and S. Balasubramanian, *Biochemistry*, 2006, **45**, 7854–7860.
24 A. T. Phan, V. Kuryavyi, S. Burge, S. Neidle and D. J. Patel, *J. Am. Chem. Soc.*, 2007, **129**, 4386–4392.
25 A. Terenzi, A. Lauria, A. M. Almerico and G. Barone, *Dalton Trans.*, 2015, **44**, 3527–3535.
26 A. Terenzi, R. Bonsignore, A. Spinello, C. Gentile, A. Martorana, C. Ducani, B. Högberg, A. M. Almerico, A. Lauria and G. Barone, *RSC Adv.*, 2014, **4**, 33245–33256.
27 A. De Cian, L. Guittat, M. Kaiser, B. Saccà, S. Amrane, A. Bourdoncle, P. Alberti, M.-P. Teulade-Fichou, L. Lacroix and J.-L. Mergny, *Methods*, 2007, **42**, 183–195.
28 N. H. Abd Karim, O. Mendoza, A. Shivalingam, A. J. Thompson, S. Ghosh, M. K. Kuimova and R. Vilar, *RSC Adv.*, 2014, **4**, 3355–3363.
29 A. A. Coelho, *J Appl Crystallogr*, 2018, **51**, 210–218.
30 D. Renčiuk, J. Zhou, L. Beaurepaire, A. Guédin, A. Bourdoncle and J.-L. Mergny, *Methods*, 2012, **57**, 122–128.
31 A. Wolfe, G. H. Shimer and T. Meehan, *Biochemistry*, 1987, **26**, 6392–6396.
32 M. J. Frisch, G. W. Trucks, H. B. Schlegel, G. E. Scuseria, M. A. Robb, J. R. Cheeseman, G. Scalmani, V. Barone, G. A. Petersson, H. Nakatsuji, X. Li, M. Caricato, A. V. Marenich, J. Bloino, B. G. Janesko, R. Gomperts, B. Mennucci, H. P. Hratchian, J. V. Ortiz, A. F. Izmaylov, J. L. Sonnenberg, D. Williams-Young, F. Ding, F. Lipparini, F. Egidi, J. Goings, B. Peng, A. Petrone, T. Henderson, D. Ranasinghe, V. G. Zakrzewski, J. Gao, N. Rega, G. Zheng, W. Liang, M. Hada, M. Ehara, K. Toyota, R. Fukuda, J. Hasegawa, M. Ishida, T. Nakajima, Y. Honda, O. Kitao, H. Nakai, T. Vreven, K. Throssell, J. A. Montgomery Jr., J. E. Peralta, F. Ogliaro, M. J. Bearpark, J. J. Heyd, E. N. Brothers, K. N. Kudin, V. N. Staroverov, T. A. Keith, R. Kobayashi, J. Normand, K. Raghavachari, A. P. Rendell, J. C. Burant, S. S. Iyengar, J. Tomasi, M. Cossi, J. M. Millam, M. Klene, C. Adamo, R. Cammi, J. W. Ochterski, R. L. Martin, K. Morokuma, O. Farkas, J. B. Foresman and D. J. Fox, Gaussian, Inc., Wallingford CT, 2016.
33 Y. Wang, X. Jin, H. S. Yu, D. G. Truhlar and X. He, *Proc. Natl. Acad. Sci. U.S.A.*, 2017, **114**, 8487–8492.
34 A. W. Ehlers, M. Böhme, S. Dapprich, A. Gobbi, A. Höllwarth, V. Jonas, K. F. Köhler, R. Stegmann, A. Veldkamp and G. Frenking, *Chemical Physics Letters*, 1993, **208**, 111–114.

35 R. Krishnan, J. S. Binkley, R. Seeger and J. A. Pople, *The Journal of Chemical Physics*, 1980, **72**, 650–654.
36 G. M. Morris, R. Huey, W. Lindstrom, M. F. Sanner, R. K. Belew, D. S. Goodsell and A. J. Olson, *J. Comput. Chem.*, 2009, **30**, 2785–2791.
37 E. F. Pettersen, T. D. Goddard, C. C. Huang, E. C. Meng, G. S. Couch, T. I. Croll, J. H. Morris and T. E. Ferrin, *Protein Science*, 2021, **30**, 70–82.
38 T. Mosmann, *Journal of immunological methods*, 1983, **65**, 55–63.
39 A. Lauria, A. Alfio, R. Bonsignore, C. Gentile, A. Martorana, G. Gennaro, G. Barone, A. Terenzi and A. M. Almerico, *Bioorganic & Medicinal Chemistry Letters*, 2014, **24**, 3291–3297.